

# Magnetic field tuning of spin resonance in TmFeO<sub>3</sub> single crystal probed with THz transient

Jiajia Guo<sup>1</sup>, Long Cheng<sup>2</sup>, Zhuang Ren<sup>2</sup>, Wenjie Zhang<sup>1</sup>, Xian Lin<sup>1</sup>, Zuanming Jin<sup>1</sup>, Shixun Cao<sup>1,3</sup>, Zhigao Sheng<sup>2,3</sup> and Guohong Ma<sup>1,3</sup>

<sup>1</sup> Department of Physics, College of Science, Shanghai University, Shanghai 200444, People's Republic of China

<sup>2</sup> Anhui Key Laboratory of Condensed Matter Physics at Extreme Conditions, High Magnetic Field Laboratory, Chinese Academy of Sciences, Hefei 230031, People's Republic of China

E-mail: [phymagh@shu.edu.cn](mailto:phymagh@shu.edu.cn) (G Ma), [zhigaosheng@hmfl.ac.cn](mailto:zhigaosheng@hmfl.ac.cn) (Z Sheng) and [sxcao@shu.edu.cn](mailto:sxcao@shu.edu.cn) (S Cao)

Received 24 September 2019, revised 12 December 2019

Accepted for publication 17 January 2020

Published 6 February 2020



## Abstract

TmFeO<sub>3</sub>, a canted antiferromagnet, has two intrinsic spin resonance modes in the terahertz (THz) frequency regime: quasi-ferromagnetic (q-FM) mode and quasi-antiferromagnetic (q-AFM) mode. Both the q-FM and q-AFM modes show strong magnetic field and temperature dependence. Hereby, by employing THz time-domain spectroscopy combined with external magnetic field and low temperature system, we systematically investigated the magnetic field induced frequency shift of q-FM and q-AFM modes as well as the temperature driven spin reorientation phase transition in TmFeO<sub>3</sub> single crystal. In contrast to the isotropic temperature dependent two-mode, the magnetic field dependence of two-mode is strongly anisotropic: the magnetic field applied along *c*-axis (*a*-axis) can harden (soften) the spin resonance frequency of q-FM mode for  $\Gamma_4$  phase of TmFeO<sub>3</sub>, and the field applied along *b*-axis shows negligible frequency shift for the q-FM mode, with the q-AFM mode relatively stable. The present study provides solid evidence that the magnetic anisotropy in rare earth orthoferrite plays a dominant role in the q-FM mode and the occurrence of spin reorientation phase transition. With the magnetic anisotropic energy obtained from the temperature dependent q-FM and q-AFM mode frequencies, we can predict both magnetic field and temperature dependence of spin resonance in TmFeO<sub>3</sub> single crystal via phenomenological analysis.

Keywords: spin resonance, orthoferrite, terahertz spectroscopy, magnetic anisotropic, spin reorientation phase transition

(Some figures may appear in colour only in the online journal)

## 1. Introduction

Ultrafast control of spin has attracted significant attention from researchers because of its importance in spintronics and spin-based information processing [1, 2]. Recently, rare earth orthoferrites (RFeO<sub>3</sub>, with R denoting Y and rare earth elements) have been gained intensive interest thanks

to their exotic magnetic properties, multiferroics and promising applications in ultrafast spin switching and photomagnetic recording, etc [3–7]. The RFeO<sub>3</sub> family has the distorted perovskite structure with the space group  $D_{2h}^{16}$ -Pbnm and possess two magnetic ions, rare earth  $R^{3+}$  and iron  $Fe^{3+}$  ions [8–10]. Due to the antisymmetric Dzyaloshinsky–Moriya (DM) interaction, the iron spin directions are not completely collinear but are slightly canted with respect to one another and then induce a weak macroscopic magnetization [11, 12].

<sup>3</sup> Author to whom any correspondence should be addressed.

The magnetic response of the  $\text{RFeO}_3$  can be well described by two-spin-sublattice model, in which two  $\text{Fe}^{3+}$  spins,  $\mathbf{S}_1$  and  $\mathbf{S}_2$ , are anti-parallel but canted along  $c$ -( $a$ -) axis for  $\Gamma_4$  ( $\Gamma_2$ ) phase [13]. Usually, two vectors  $\mathbf{F} = \mathbf{S}_1 + \mathbf{S}_2$  and  $\mathbf{G} = \mathbf{S}_1 - \mathbf{S}_2$  are introduced to describe the magnetic response upon external stimuli. Previous researches also proved that the properties of orthoferrites are sensitive to temperature, pressure, and magnetic field, and evoke a series of intriguing order–disorder transitions [14–22]. The underlying mechanism and possible modulation of these transitions will provide deeper insights into design of novel spintronic devices [15].

Terahertz time-domain spectroscopy (THz-TDS) has emerged as an alternative to optical spectroscopy for studying magnetic excitation without unavoidable excessive thermal energy due to the very low photon energy (1 THz–4.1 meV) [23–25]. The magnetic interaction between THz pulse and  $\text{RFeO}_3$  can be described with the Zeeman torque  $\mathbf{T} = \gamma \mathbf{S} \times \mathbf{H}_{\text{THz}}$ , where  $\gamma$  is the gyromagnetic ratio,  $\mathbf{S}$  and  $\mathbf{H}_{\text{THz}}$  are the electron's spin moment and the impulsive magnetic field of the incident THz pulse, respectively [26, 27]. After the magnetic moment being tipped out of easy direction by  $\mathbf{T}$ , the spins start to precess around the effective magnetic field. The induced precession is expected to radiate free induction decay (FID) signal. The amplitude of the FID signal is proportional to magnetic torque  $\mathbf{T}$ , and the resonant frequency of polarized electromagnetic wave is equal to the precession frequency of the spins [28]. Below Néel temperature and above spin reorientation phase transition temperature without external fields, the magnetic structure of  $\text{RFeO}_3$  corresponds to the  $\Gamma_4$  phase ( $G_x, F_z$ ) with a weak ferromagnetic moment  $\mathbf{F}$  along the  $c$ -axis and the antiferromagnetic vector  $\mathbf{G}$  along the  $a$ -axis [29]. Usually, with variations of temperature or (and) magnetic field, the sample system is transferred into another configuration  $\Gamma_2$  ( $F_x, G_z$ ) with  $\mathbf{F}$ // $a$ -axis and  $\mathbf{G}$ // $c$ -axis.

In this paper, we focus our investigation on the frequency shift of quasi-ferromagnetic (q-FM) and quasi-antiferromagnetic (q-AFM) modes induced by the external magnetic field in  $\text{TmFeO}_3$  single crystal by using THz-TDS. We discuss the strongly anisotropic of the magnetic field dependent spin resonance with the applied magnetic field along different crystal axis. Furthermore, on the basis of the magnetic anisotropy energies estimated according to the temperature dependent resonant frequencies, we can predict both magnetic field and temperature dependence of spin resonance in  $\text{TmFeO}_3$ . These results can be generally applicable for other  $\text{RFeO}_3$  members.

## 2. Sample details and experimental setup

Our  $\text{TmFeO}_3$  single crystal was grown by the optical-floating-zone method (Crystal System Inc., type FZ-T-10000-H-VI-P-SH, Crystal System Corp). The samples with  $a$ -,  $b$ - and  $c$ -cut plane parallel plates, having thickness of 1.16, 0.89 and 1.31 mm respectively, were polished on both sides for THz measurements. The directions of the crystal axis were determined by the x-ray Laue diffraction analysis. The THz-TDS integrated with the strong-magnetic field and a low-temperature system was used for the TDS measurement. The second

harmonic output of Erbium-doped femtosecond fiber laser (C-Fiber-780-High-Power, Menlo Systems) with a centered wavelength of 780 nm, pulse duration of 90 fs and repetition rate of 100 MHz was used to generate and detect the THz transients. The emitter and detector of the THz pulses were achieved by photoconductive antennas. The sample was mounted in the Oxford Instruments Spectromag He-bath cryostat (SHC) placed in a collimated terahertz beam. The temperature ranges from 40 to 300 K, and the magnetic field is up to the maximum value of 7.0 T. The effective spectral range of the THz pulse covers the range from 0.1 to 1.5 THz.

Considering the low signal to noise ratio in the THz-TDS system loaded with high magnetic field system, we also studied the spin resonance of  $\text{TmFeO}_3$  crystal in a home-made THz-TDS system without magnetic field. Briefly, the output of a mode-locked Ti: Sapphire laser, with pulse duration of 100 fs, centered wavelength of 800 nm, and repetition rate of 80 MHz (Mai Tai HP-1020, Spectra-Physics), is used to generate and detect the THz transient. The emitter and detector of the THz wave were photoconductive antennas fabricated on low-temperature-grown GaAs substrate, and the effective THz spectral range covers the range from 0.1 to 3.0 THz. The sample is installed in a cold finger cryostat with two THz transparent windows, of which the temperature is tunable in a range from 40 to 300 K with best resolution of 1 K. The THz spectrometer was purged with nitrogen to avoid THz absorption of atmospheric water vapor. The THz-TDS allows us to measure the temperature dependence of FID signals with the S/N ratio better than 5000:1, from which we can obtain the temperature induced spin reorientation transition (SRT), as well as analyze the polarization state of the FID.

## 3. Results and discussions

The  $\text{Fe}^{3+}$  spins in  $\text{TmFeO}_3$  order antiferromagnetically below Néel Temperature ( $T_N = 650$  K for  $\text{TmFeO}_3$ ). At temperatures above 93 K and below Néel temperature, the crystal is in the  $\Gamma_4$  phase, in which the spins of the two  $\text{Fe}^{3+}$  sublattice are antiparallel along the  $a$ -axis but canted towards the  $c$ -axis by a small angle ( $\sim 8$  mrad). The crystal is transformed in the  $\Gamma_2$  phase when the temperature is below 83 K, in which the weak ferromagnetic moment  $\mathbf{F}$  is pointed along  $a$ -axis. During 93 and 83 K, the crystal is in the  $\Gamma_{24}$  phase, in which the weak ferromagnetic moment  $\mathbf{F}$  lies in ( $ac$ ) plane of the crystal. There are two spin resonance modes in THz frequency, q-FM mode and q-AFM mode, which modes can be selectively excited with magnetic component ( $\mathbf{H}_{\text{THz}}$ ) of incident THz pulse perpendicular or parallel to the ferromagnetic moment,  $\mathbf{F}$ , of the crystal, respectively.

### 3.1. The assignment of the resonance modes

Figures 1(a) and (b) plot the 3D trajectories of electric field for q-FM (a) and q-AFM (b) modes of  $\text{TmFeO}_3$  single crystal at room temperature, respectively. It is clearly seen that the FID signal for q-FM mode shows a nearly circular polarization, while that of q-AFM mode shows a linear polarization.

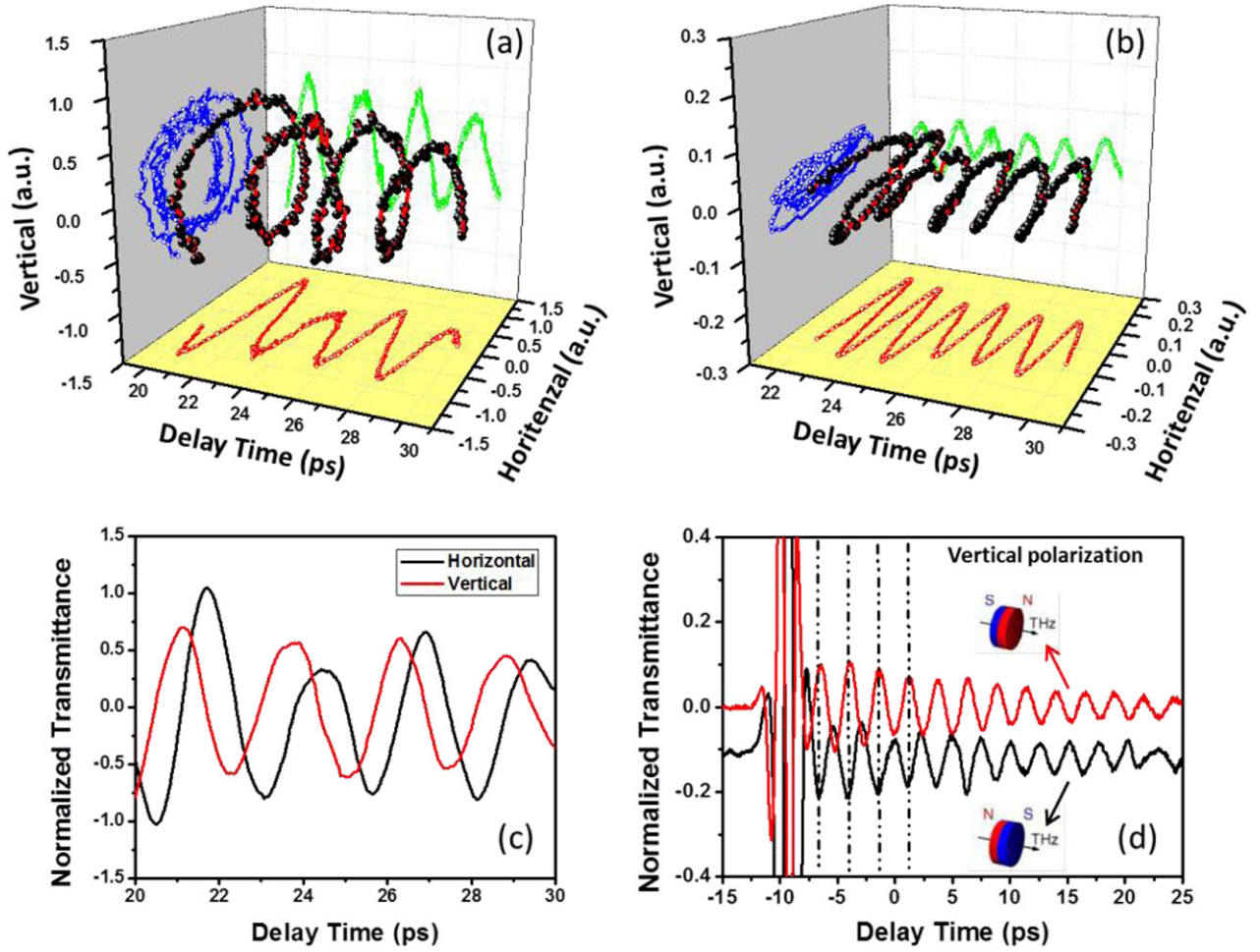


**Figure 1.** (a) The 3D plots of the horizontal and the vertical THz electric field component of the q-FM mode. (b) The 3D plots of the horizontal and the vertical THz electric field component of the q-AFM mode. (c) The horizontal (black) and vertical (red) polarizations of q-FM mode. (d) The FID signals of the vertical components for the THz pulse propagating parallel (red) and antiparallel to the magnetic moment vector  $\mathbf{F}$ .

The polarization of the FID signal is evaluated by inserting a THz polarizer at the polarization angles of  $\pm 45^\circ$  with respect to the horizontal direction. The sum and difference of these two spectra at  $\pm 45^\circ$  give the horizontal and vertical electric field components, respectively. The q-FM mode with circular polarization is due to the precession of macro magnetization around equilibrium position, while the linear polarization of q-AFM is understood as the in-plane vibration of the macro magnetization. The derivation of circular polarization for q-FM mode may come from the anisotropy of the crystal in orthogonal direction, i.e. the THz refractive indices are different for horizontal and vertical directions, and the same reason is applicable for the deviation of perfectly linear polarization for q-AFM mode. Figure 1(c) plots the horizontal and vertical polarizations together for direct comparison, from which we can see more clearly that the horizontal and vertical polarizations have  $\pi/2$  phase shift with comparable amplitude. Figure 1(d) shows the vertical polarization of q-FM mode, in which THz is propagating parallel (red) and antiparallel (black) to the magnetic moment vector  $\mathbf{F}$ . It can be found that the FID signals of vertical components show out-of-phase for the two opposite propagation directions of THz pulse. This

incident THz direction dependence of FID signals manifests the resonance mode is magnetic in nature.

### 3.2. Temperature dependent spin resonance

Before studying the magnetic field dependence of spin resonance, we would like to discuss the temperature dependent spin resonance. As reported previously in [30], the q-AFM mode frequency changes slightly with temperature, in contrast, the q-FM mode frequency alters significantly near the SRT temperature. The spin resonance frequency is related to the magnetic anisotropy constant in the  $ac$ -plane, which can be described by [31, 32]

$$(\hbar\omega_{\text{FM}})^2 = \left[ \frac{4E}{(2S)^2} \right] [(A_{xx} - A_{zz}) \cos 2\theta - 4K_4 \cos 4\theta] \quad (1)$$

$$(\hbar\omega_{\text{AFM}})^2 = \left[ \frac{4E}{(2S)^2} \right] \left[ \frac{1}{2} (A_{xx} + A_{zz}) + \frac{1}{2} (A_{xx} - A_{zz}) \cos 2\theta - K_4 \cos 4\theta \right], \quad (2)$$



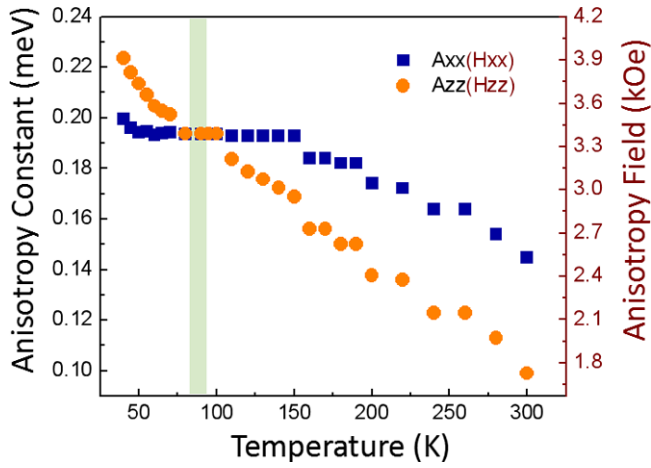


**Figure 2.** The calculated magnetic anisotropy constants  $A_{xx}$  and  $A_{zz}$  in the  $ac$ -plane as a function of temperature according to equations (1) and (2).  $A_{xx}$  and  $A_{zz}$  denote the magnetocrystalline anisotropic constant along  $x(a)$  and  $z(c)$  axis, respectively. The red scale on the right indicates the estimated magnetic anisotropy fields  $H_{xx}$  and  $H_{zz}$  according to  $A_{xx}$  and  $A_{zz}$ . The shadow area shows the SRT temperature range.

where  $\omega_{\text{FM}}$  and  $\omega_{\text{AFM}}$  denote the angular frequency of q-FM and q-AFM modes, respectively.  $\hbar$  is the reduced Planck constant, and  $\theta$  is the angle between the  $c$ -axis and the weak ferromagnetic moment  $\mathbf{F}$ ,  $E = 373$  meV is the exchange constant [31],  $S = 5/2$  is spin quantum number in the  $\text{Fe}^{3+}$  ion sublattice,  $A_{xx}$  and  $A_{zz}$  are the magnetic anisotropy constants along  $x(a)$  and  $z(c)$  axis of the crystal, and the higher-order anisotropy constant  $K_4$  is much smaller than those of  $A_{xx}$  and  $A_{zz}$ , which can be neglected during calculations of the magnetic anisotropy energy for simplicity. With the q-FM and q-AFM frequencies in  $\text{TmFeO}_3$  single crystal under various temperatures [30], the temperature-dependent magnetic anisotropy constants are obtained according to equations (1) and (2), which is presented in figure 2. It is seen that the magnetic anisotropy constants,  $A_{xx}$  and  $A_{zz}$ , are strongly temperature dependent. The estimated magnetic anisotropy fields  $H_{xx}$  and  $H_{zz}$  according to the anisotropy constants,  $A_{xx}$  and  $A_{zz}$  are also given in figure 2 with red scale. We will use the measured temperature dependent anisotropic energy to fit the magnetic field dependence of spin resonance in the following part.

### 3.3. Magnetic field dependent spin resonance

Figure 3(a) shows the THz transmission spectra of  $c$ -cut  $\text{TmFeO}_3$  crystal under various magnetic fields applied along  $c$ -axis at 150 K, i.e. the magnetic field up to 7 T is applied  $c$ -axis, the propagation direction of probing THz pulse. The polarization of probing THz pulse is set along  $b$ -axis of the crystal (magnetic component of THz pulse,  $\mathbf{H}_{\text{THz}}$ , is along  $a$ -axis). At 150 K, the  $\text{TmFeO}_3$  crystal is in the  $\Gamma_4$  phase, and the magnetic moment is pointed along  $c$ -axis of the crystal, as a result only the q-FM mode can be excited with the magnetic component,  $\mathbf{H}_{\text{THz}}$ , of THz wave. Figure 3(b) plots the extracted q-FM resonance frequency as a function of the applied magnetic field; it is seen that the resonance frequency increases linearly with the magnitude of applied magnetic

field. We would like to mention that the q-AFM mode is inactive to incident THz pulse for the  $c$ -cut  $\text{TmFeO}_3$  at 150 K, and figure 3 only presents the experimental data of q-FM mode. According to Herrmann [33], the magnetic field dependent q-FM mode frequency can be estimated:

$$\omega_{\text{FM}}^2/\gamma^2 = \omega_{\text{FM}}^2(0)/\gamma^2 + (5H_{xz} + H_D)H + H^2 \quad (3)$$

$$\omega_{\text{AFM}}^2/\gamma^2 = \omega_{\text{AFM}}^2(0)/\gamma^2 + (H_{xz} + H_D)H. \quad (4)$$

Here,  $H_D = 185$  kOe is the antisymmetric exchange field [34],  $H_{xz}$  is the effective anisotropy fields,  $\mathbf{H}$  is the applied magnetic field along  $c$ -axis in the  $\Gamma_4$  phase (or along  $a$ -axis in the  $\Gamma_2$  phase [35]),  $\omega_{\text{FM}}(0)$  and  $\omega_{\text{AFM}}(0)$  are the angular frequency of q-FM and q-AFM modes without external magnetic field, and  $\gamma = 1.86 \times 10^7 \text{ s}^{-1} \text{ Oe}^{-1}$  is the gyromagnetic ratio [36]. The magnitude of magnetic anisotropy field  $H_{xz}$  is in the order of a few kOe, which is two-order smaller than that of  $H_D$ . The solid green line in figure 3(b) shows the fitting results based on equations (3) and (4) with  $H_{xz} = 0$ . The red line is the best fitting with an adjustable constant  $H_{xz}$ , which produces  $H_{xz} = 1.85$  kOe. We assume that all anisotropic energies,  $A_{xx}$ ,  $A_{zz}$ ,  $A_{xz}$  and  $A_{xy}$ , are only temperature dependent, and independent on the external magnetic field.

Figures 4(a) and (c) show the THz transmission spectra of  $b$ -cut  $\text{TmFeO}_3$  under various magnetic fields applied along  $b$ -axis of the crystal at 150 K. In figure 4(a) the  $\mathbf{H}_{\text{THz}}$  of incident THz pulse is set along  $a$ -axis, so that q-FM mode is excited under this configuration. In figure 4(c) the  $\mathbf{H}_{\text{THz}}$  of incident THz pulse is set along  $c$ -axis, so that q-AFM mode is excited under this configuration. Figures 4(b) and (d) plot the q-FM mode and q-AFM mode frequency respectively versus applied magnetic field. It is seen that the magnetic field along the crystal  $b$ -axis does not alter the q-FM mode frequency apparently up to 7 T, and the q-AFM mode frequency slightly increases with the magnitude of applied magnetic field. According to [33], when the external magnetic field is applied along  $b$ -axis of the crystal for both  $\Gamma_4$  and  $\Gamma_2$  phases, the magnetic field dependent q-FM mode and q-AFM mode frequency can be described by:

$$\omega_{\text{FM}}^2/\gamma^2 = \omega_{\text{F}}^2(0)/\gamma^2 - \frac{4H_{xz}^2}{4H_{zz}H_E + (H_D + H_{xz})(H_D - 3H_{xz})}H^2 \quad (5)$$

$$\omega_{\text{AFM}}^2/\gamma^2 = \omega_{\text{AF}}^2(0)/\gamma^2 + \frac{4H_{zz}H_E + (H_D - H_{xz})^2}{4H_{zz}H_E + (H_D + H_{xz})(H_D - 3H_{xz})}H^2 \quad (6)$$

here,  $H_E = 6400$  kOe is the effective symmetric exchange field [34]. It is noted that the  $H_{xz}$  and  $H_{zz}$  have the similar order of magnitude, and both of them are two-order smaller than that of  $H_D$  and  $H_E$ , and the applied magnetic field,  $\mathbf{H}$ , is one-order of magnitude smaller than that of  $H_D$  and  $H_E$ , therefore the second terms on the right hand of equation (5) are close to zero for our case  $\mathbf{H} \leq 7$  T. It should be noted that the second term on the right hand of equation (6) can not be ignored, and consider much smaller magnitude of  $H_{zz}$  than that of  $H_D$  and  $H_E$ , the frequency of q-AFM mode is approximately proportional to the square of the magnetic field applied along  $b$ -axis of the crystal.

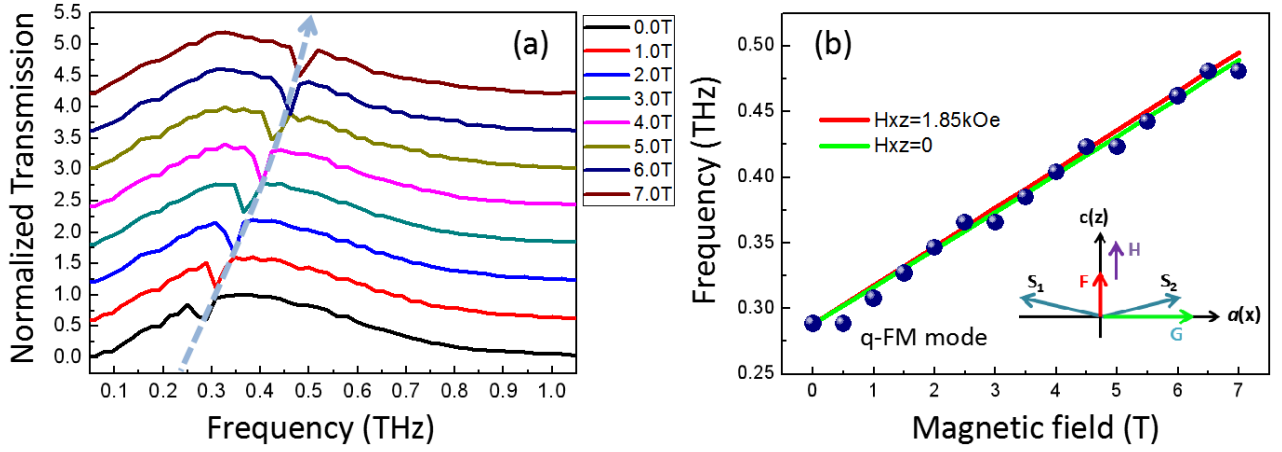


**Figure 3.** (a) THz transmission spectra of *c*-cut TmFeO<sub>3</sub> under various magnetic field at 150 K. The incident THz magnetic component,  $\mathbf{H}_{\text{THz}}$ , is aligned along *a*-axis of the crystal, and the external magnetic field  $\mathbf{H}$  up to 7 T is applied along *c*-axis of the crystal. The offset of adjacent lines is incremented by 0.6 for clarity. (b) The q-FM mode frequency is plotted as a function of applied magnetic field. The solid lines are fitting lines with  $H_{xz} = 1.85 \pm 0.25 \text{ kOe}$  (red) and  $H_{xz} = 0$  (green) based on the equation (3) in the text. The inset in (b) shows the schematics of the simplified magnetic configuration in TmFeO<sub>3</sub> with  $\Gamma_4$  phase.

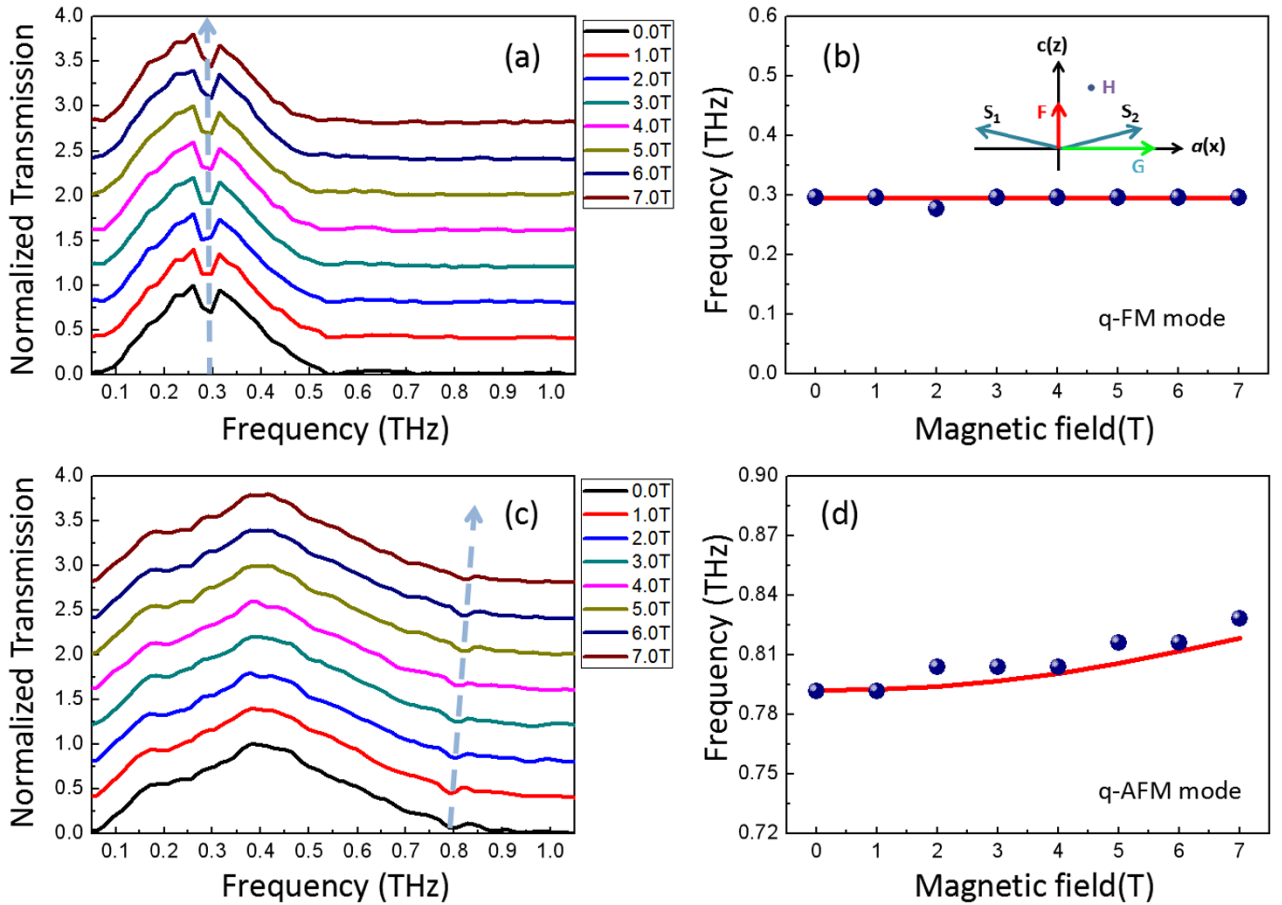


**Figure 4.** THz transmission spectra of *b*-cut TmFeO<sub>3</sub> under various magnetic field at 150 K. (a) The incident THz magnetic component,  $\mathbf{H}_{\text{THz}}$ , is aligned along *a*-axis of the crystal, and the external magnetic field  $\mathbf{H}$  up to 7 T is applied along *b*-axis of the crystal. The offset of adjacent lines is incremented by 0.4. (b) The q-FM mode frequency extracted from (a) is plotted as a function of magnetic field. (c) The incident THz magnetic component,  $\mathbf{H}_{\text{THz}}$ , is aligned along *c*-axis of the crystal, and the external magnetic field  $\mathbf{H}$  up to 7 T is applied along *b*-axis of the crystal. The offset of adjacent lines is incremented by 0.4. (d) The q-AFM mode frequency extracted from (c) is plotted as a function of magnetic field. The solid is the fitting curve with fitting parameters given in text. The inset in (b) shows the schematics of the simplified magnetic configuration in a  $\Gamma_4$  phase TmFeO<sub>3</sub>.

Figure 5 presents both q-FM and q-AFM modes as a function of magnetic field applied along the *a*-axis of the crystal. Figure 5(a) shows the THz transmission spectra of *c*-cut

TmFeO<sub>3</sub> with magnetic field up to 7 T applied along *a*-axis at 150 K. The  $\mathbf{H}_{\text{THz}}$  of THz pulse is aligned along *b*-axis so that only q-FM mode can be excited with this configuration,

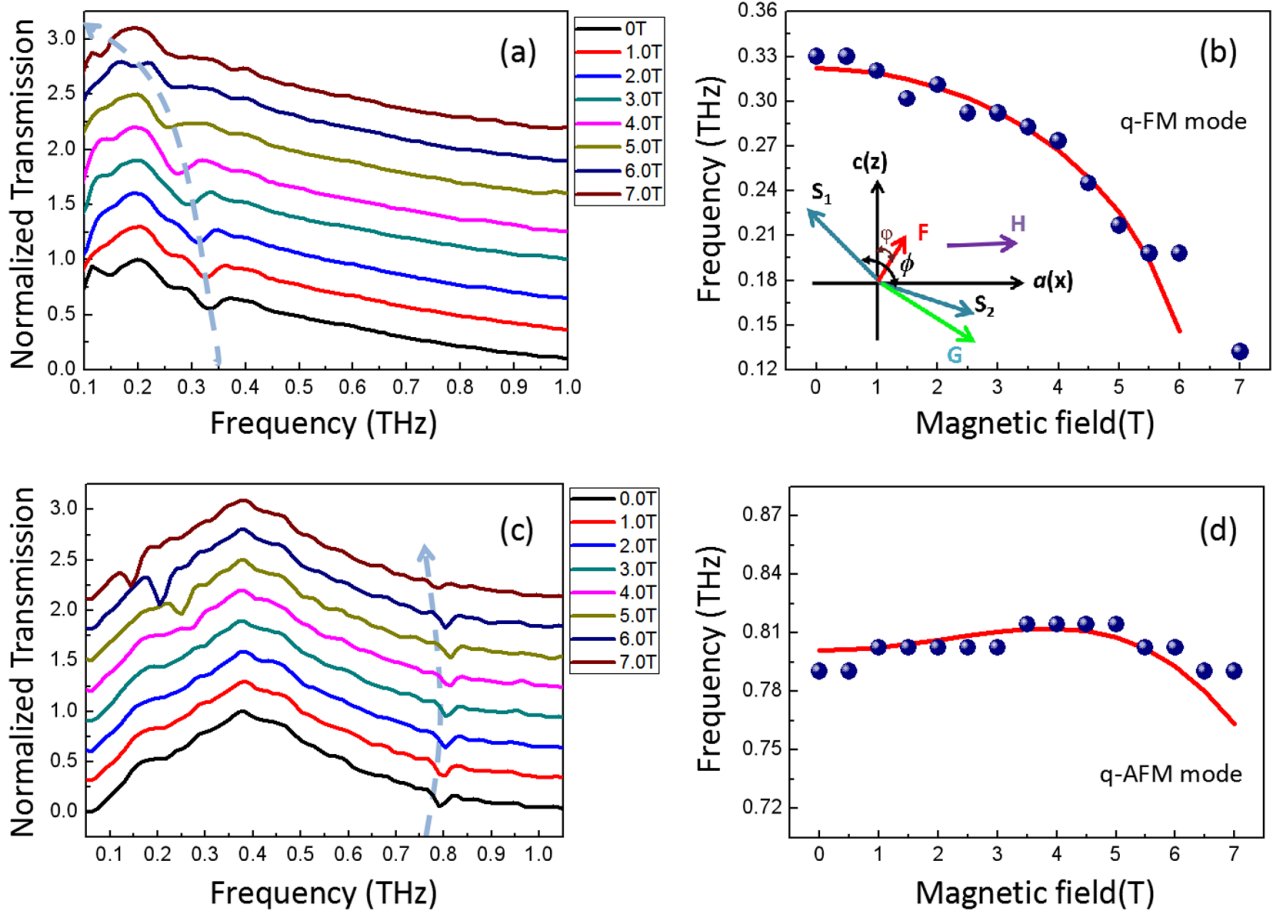


**Figure 5.** (a) THz transmission spectra of *c*-cut TmFeO<sub>3</sub> under various magnetic fields at 150 K. The incident THz magnetic component,  $\mathbf{H}_{\text{THz}}$ , is aligned along *b*-axis of the crystal, and the external magnetic field  $\mathbf{H}$  up to 7 T is applied along *a*-axis of the crystal. The offset of adjacent lines is incremented by 0.3. (b) The extracted q-FM mode frequency from (a) is plotted as a function of magnetic field. (c) THz transmission spectra of *a*-cut TmFeO<sub>3</sub> under various magnetic fields at 150 K. The incident THz magnetic component,  $\mathbf{H}_{\text{THz}}$ , is aligned along *c*-axis of the crystal, and the external magnetic field  $\mathbf{H}$  up to 7 T is applied along *a*-axis of the crystal. The offset of adjacent lines is incremented by 0.3. (d) The extracted q-AFM mode frequency extracted from (c) is plotted as a function of magnetic field. The solid line is the fitting curve. The inset in (b) shows the schematics of the simplified magnetic configuration in TmFeO<sub>3</sub>.  $\mathbf{S}_1$  and  $\mathbf{S}_2$  stand for two pairs of spins for Fe<sup>3+</sup> sublattices.

and figure 5(c) shows the THz transmission spectra of *a*-cut TmFeO<sub>3</sub> with magnetic field up to 7 T applied along *a*-axis at 150 K. The  $\mathbf{H}_{\text{THz}}$  of THz pulse is pointed along *a*-axis so that the q-AFM mode can be excited with this configuration. It is clearly seen that the q-FM mode frequency decreases with the magnitude of applied magnetic field, while the q-AFM mode frequency shows negligible shift. Figures 5(b) and (d) show the extracted q-FM mode frequency and q-AFM mode frequency with respect to the applied magnetic field, respectively. When the magnetic field is applied perpendicularly to the magnetic moment  $\mathbf{F}$ , it is possible that the applied field can rotate the magnetic moment  $\mathbf{F}$  in the *ac* plane of the crystal. As a result, this situation is much more complex than the two cases mentioned before (magnetic field is applied along *c*-axis (figure 3) and *b*-axis (figure 4), respectively).

In order to reproduce the magnetic field dependence of q-FM mode for this situation, the inset in figure 5(b) schematically shows the rotation of magnetic moment induced by external magnetic field. Here,  $\phi$  describes the angle between the vector  $\mathbf{F}$  and *c*-axis, which becomes larger with the increase of the magnetic field applied along *a*-axis of the

crystal.  $\phi$  denotes the angle between the two spin sublattices  $\mathbf{S}_1$  and  $\mathbf{S}_2$ , which becomes smaller as the increase of the applied magnetic field. If the applied magnetic field is lower than a critical field,  $\mathbf{H}_{\text{cr}}$ , i.e.  $\mathbf{H} \leq \mathbf{H}_{\text{cr}}$ , the angle  $\phi$  of the canted phase is governed by [37]

$$H_E H_{A2} \sin^3 \phi + (H_E H_{xz} - \eta H^2) \sin \phi - H H_D = 0 \quad (7)$$

where  $H_{A2}$  is the effective biquadratic anisotropy field in *ac*-plane, and  $\eta = (\chi_{\perp} - \chi_{\parallel})/\chi_{\perp}$ ,  $\chi_{\perp}$  and  $\chi_{\parallel}$  are the longitudinal and transverse antiferromagnetic susceptibilities, respectively. It should be noticed that the  $H_{xz}$  in equation (7) can not be ignored at this condition. The dynamical spin response can be obtained by solving a Landau–Lifshitz–Gilbert equation [38, 39], and the relationship between the frequencies of q-FM and q-AFM modes and the applied magnetic field  $\mathbf{H}$  can be written as [39]

$$\frac{2\omega_{\text{FM,AFM}}^2}{\gamma^2} = P + Q + R \mp [(P - Q + R)^2 + 4QR]^{1/2} \quad (8)$$

where

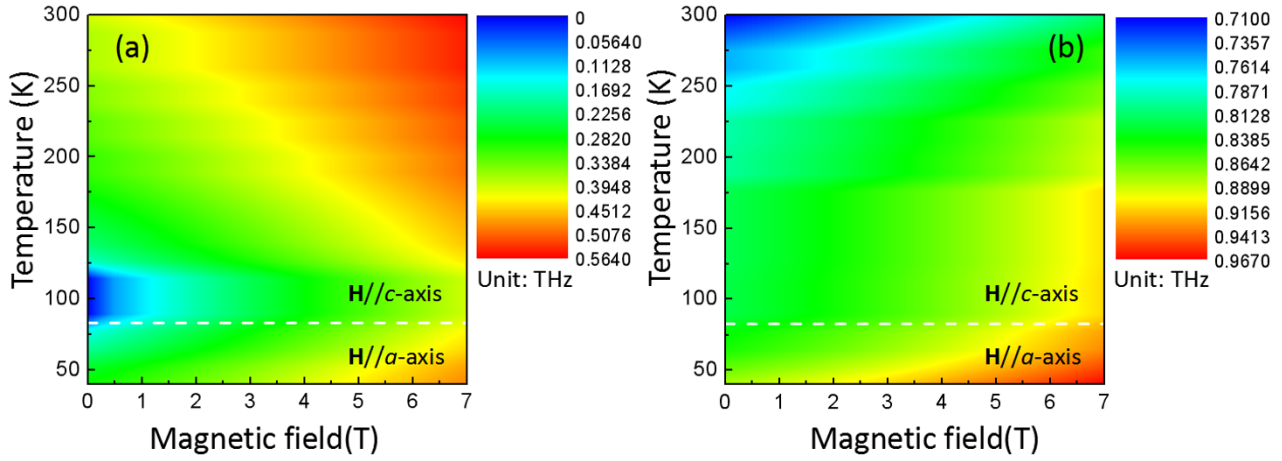


**Figure 6.** The resonance frequency mapping of (a) q-FM mode and (b) q-AFM mode in TmFeO<sub>3</sub> single crystal as functions of both temperature and the external magnetic field applied along *c*-axis above 83 K and along *a*-axis below 83 K. The resonance frequencies (both q-FM and q-AFM) are shown with different colors with the unit of THz.

$$\begin{cases} P = H_E H_{xy} + H_D^2 - \eta H^2 \\ Q = H_E (H_{xz} + 3H_{A2} \sin^2 \varphi) \cos^2 \varphi + H^2 (\sin^2 \varphi - \eta) \\ R = H^2 (1 + \eta)^2 \cos^2 \varphi \end{cases} \quad (9)$$

The solid lines in figures 5(b) and (d) show the best fitting of the q-FM mode and the q-AFM mode with respect to the applied magnetic field along the *a*-axis at 150 K based on equation (8). The fitting parameters used here are  $\eta = 0.7$ ,  $H_{xz} = 1.85$  kOe,  $H_{xy} = 6.1$  kOe,  $H_{A2} = 0.4$  kOe, respectively. It can be seen from figure 5(b) that the simulation based on equation (8) can reproduce the experimental data well as the magnetic field  $\mathbf{H}$  is smaller than 5 T; when the magnitude of  $\mathbf{H}$  is higher than 5 T, the fitting curve deviates from the experimental data significantly. As we can find in figure 5(c) that the q-FM mode appears with  $\mathbf{H}$  is up to 5 T, from which we can estimate the  $\mathbf{H}_{cr} \approx 5$  T. The critical magnetic field  $\mathbf{H}_{cr}$  denotes the critical point, in which the SRT starts to appear. Higher magnetic fields with larger deviation means the crystal has entered into the SRT regime, i.e. the crystal lies in  $\Gamma_{24}$  phase.

### 3.4. Both temperature and magnetic field dependent spin resonance

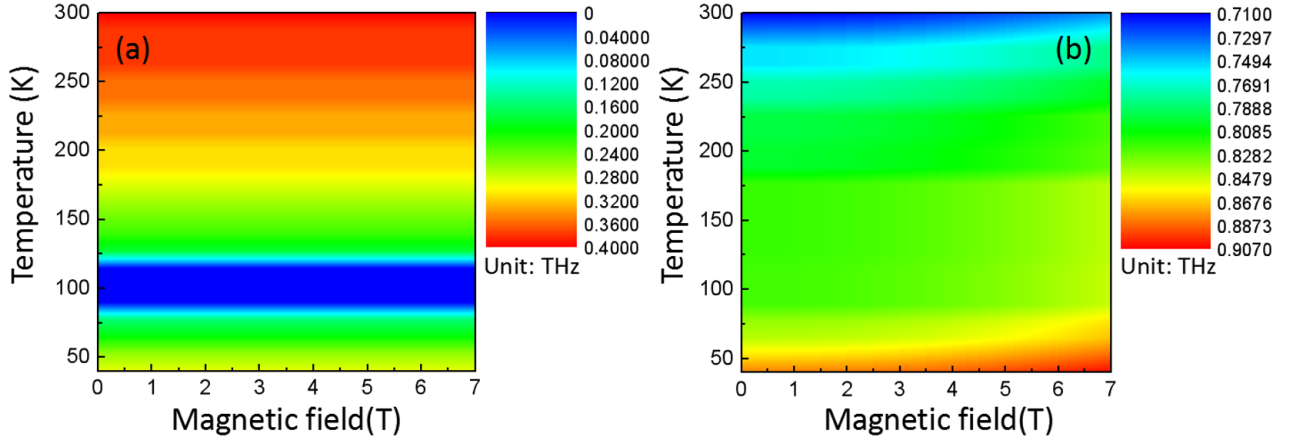
From the experimental results and discussions above, it is clear that the q-FM mode frequency is dominated by magnetic anisotropic energies that are strongly related to the temperature. The magnetic anisotropic energies  $A_{xx}$  and  $A_{zz}$  can be evaluated from the temperature dependent q-FM and q-AFM modes with the equations (1) and (2). Combined with magnetic field dependent experimental data provided in figure 3, figure 6 presents the resonance frequencies of q-FM (a) and q-AFM (b) modes in TmFeO<sub>3</sub> single crystal as functions of both temperature and the external magnetic field. It should be noticed that the magnetic field is applied along *c*-axis above 83 K, while the field is applied along *a*-axis below 83 K. The soften of q-FM resonance frequencies is seen as the temperature is approaching the SRT temperature range (83–93 K), while the resonance frequency of q-AFM mode is seen to

increase slightly with decreasing temperature. As the increase of the applied magnetic field, the frequencies of both q-FM and q-AFM modes are seen to increase. It is known that the TmFeO<sub>3</sub> lies in the  $\Gamma_{24}$  phase in the temperature interval between 93 K and 83 K without applied magnetic field. It is noted from figure 6(b) that, during the temperature interval between 93 and 83 K, the crystal could be transformed from  $\Gamma_{24}$  phase into  $\Gamma_4$  phase when the magnetic field is applied along *c*-axis. It suggests that magnetic field applied along *c*-axis of the crystal can suppress the occurrence of SRT in TmFeO<sub>3</sub>. In another word, the SRT takes place at lower temperature with a magnetic field applied along *c*-axis of the crystal.

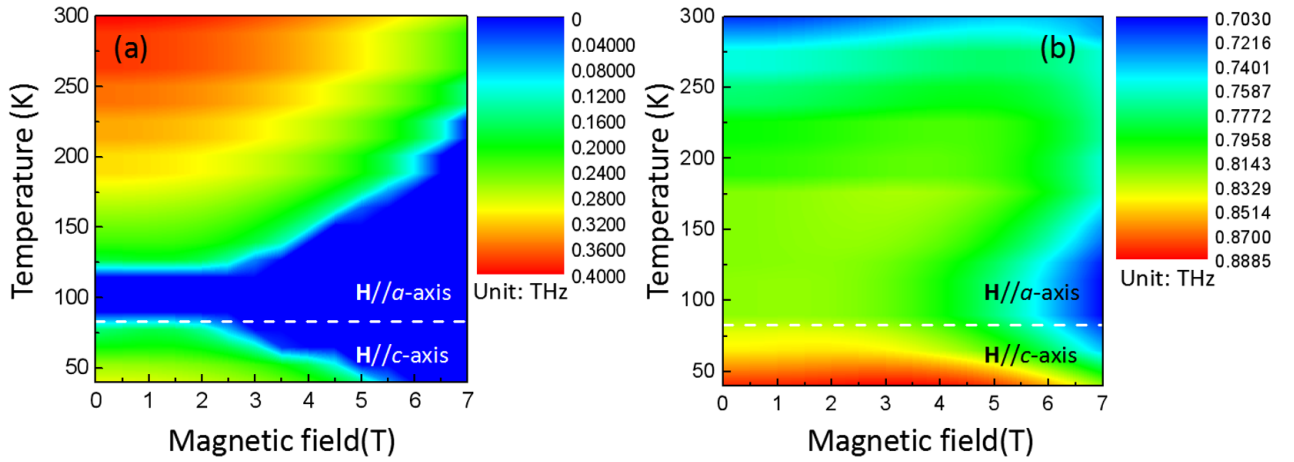
Figure 7 shows frequency mapping of the q-FM (a) and q-AFM (b) modes with respect to the temperatures as well as the magnetic field applied along *b*-axis. As shown in figure 7(a), there is a broad absorption band with the temperature below 120 K, which are assigned to the electronic transitions inside the ground multiplets of the Tm<sup>3+</sup> (<sup>6</sup>H<sub>3</sub>) at low temperature regime [30]. For a G-type antiferromagnet like TmFeO<sub>3</sub>, during the occurrence of SRT (i.e.  $\Gamma_4 \rightarrow \Gamma_{24} \rightarrow \Gamma_2$ ), the vectors  $\mathbf{F}$  and  $\mathbf{G}$  rotates in the *ac*-plane of the crystal, in which the angles  $\phi$  and  $\varphi$  remains unchanged. Under this situation, the crystal in  $\Gamma_4$  phase or in  $\Gamma_2$  phase is the same for the case of the magnetic field applied along *b*-axis of the crystal, i.e.  $\mathbf{H} // \mathbf{b}$ -axis. The frequencies of both q-FM and q-AFM modes are almost insensitive to the applied magnetic field along *b*-axis of the crystal.

Figure 8 presents the resonance frequencies of q-FM (a) and q-AFM (b) modes in TmFeO<sub>3</sub> single crystal are plotted as functions of both temperature and the external magnetic field along *a*-axis (*c*-axis) above (under) 83 K. It is seen from figure 8(a) that the frequency of q-FM mode decreases with applied magnetic field, and the mode frequency is also seen to decrease when the temperature approaches the SRT temperature interval (83–93 K). Figure 8(b) shows that the q-AFM frequency remains almost unchanged with magnetic field applied along *a*-axis (*c*-axis) of the crystal above (under) 83 K, but when the magnetic field is higher than the critical magnetic





**Figure 7.** The resonance frequency mapping of (a) FM mode and (b) AFM mode in TmFeO<sub>3</sub> single crystal as functions of both temperature and the applied magnetic field along *b*-axis. The resonance frequencies (both q-FM and q-AFM) are shown with different colors with the unit of THz.



**Figure 8.** The resonance frequency mapping of (a) q-FM mode and (b) q-AFM mode in TmFeO<sub>3</sub> single crystal as functions of both temperature and the external magnetic field applied along *a*-axis above 83 K and along *c*-axis below 83 K. The resonance frequencies (both q-FM and q-AFM) are shown with different colors with the unit of THz.

field  $\mathbf{H}_{cr}$  ( $\mathbf{H}_{cr} = 5$  T in this case), the mode frequency is seen to decrease with the increase of the applied magnetic field, which indicates the occurrence of the magnetic field induced SRT in TmFeO<sub>3</sub>. The results obtained in TmFeO<sub>3</sub> is similar to our previous experimental results in NdFeO<sub>3</sub> [20]: when the temperature is approaching the SRT temperature range, the critical magnetic field  $\mathbf{H}_{cr}$  is reduced significantly, which suggests an acceleration of SRT process in TmFeO<sub>3</sub> with an applied magnetic field along *a*-axis of the crystal.

As done in  $H_{xx}$ ,  $H_{zz}$ , we assume that the magnetic anisotropic fields  $H_{xy}$  and  $H_{xz}$  are only temperature dependent, and independent on the applied magnetic field. When the applied magnetic field is zero, i.e.  $\mathbf{H} = 0$ , and  $\varphi \approx 0$  ( $\pi/2$ ) for  $\Gamma_4$  ( $\Gamma_2$ ) phase, then the equations (8) and (9) are reduced to:

$$\omega_{FM}^2 \approx \gamma^2 H_E H_{xz} \quad (10)$$

$$\omega_{AFM}^2 \approx \gamma^2 (H_E H_{xy} + H_D^2). \quad (11)$$

Combined with the temperature dependent q-FM and q-AFM modes, the temperature dependent magnetic anisotropic fields,

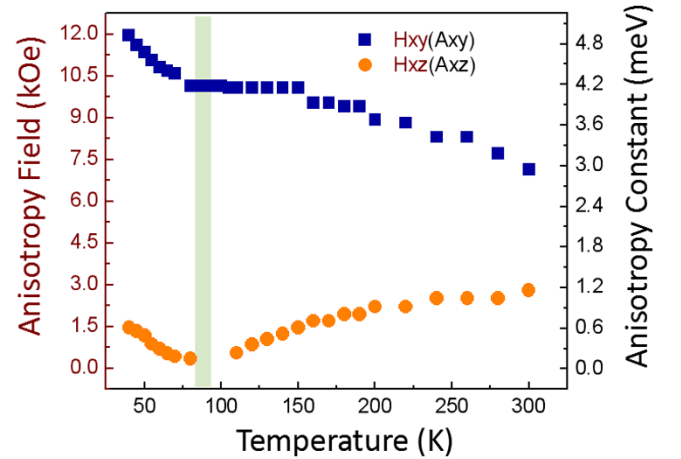


**Figure 9.** The estimated magnetic anisotropy fields  $H_{xy}$  and  $H_{xz}$  as a function of temperature according to equation (8).  $H_{xy}$  and  $H_{xz}$  denote the magnetic anisotropic field in *ab*-plane and *ac*-plane, respectively. The black scale on the right indicates the estimated magnetocrystalline anisotropy constants  $A_{xy}$  and  $A_{xz}$  according to  $H_{xy}$  and  $H_{xz}$ . The shadow area shows the SRT temperature range.



$H_{xz}$  and  $H_{xy}$  can be calculated with the equations (10) and (11), which are shown in figure 9, and the estimated magnetic anisotropy constants  $A_{xy}$  and  $A_{xz}$  are given by the black scale in figure 9. The absence of the  $A_{xz}$  in the SRT temperature interval is due to the fact that there is no observed q-FM mode frequency during this temperature range. In contrast, we can obtain the  $A_{xy}$  in the all measured temperature window. By comparing with the magnetic anisotropic constants along  $x$ -axis ( $A_{xx}$ ) and  $z$ -axis ( $A_{zz}$ ), as shown in figure 2, the magnetic anisotropic energies of  $A_{xy}$  is one order of magnitude larger than those in  $A_{xx}$ ,  $A_{zz}$  and  $A_{xz}$ .

#### 4. Conclusions

In summary, we have studied the temperature and magnetic field dependence of spin resonance in TmFeO<sub>3</sub> single crystal by using THz time-domain spectroscopy. The spin resonance frequency, particular for the case of q-FM mode, is dominated by the magnetic anisotropic energy. Our experimental results demonstrate that when the magnetic field is applied parallel to  $c$ -axis for  $\Gamma_4$  phase and parallel to  $a$ -axis for  $\Gamma_2$  phase, the both q-FM and q-AFM mode frequencies increases with the external magnetic field. On the other hand, when the magnetic field is applied along  $b$ -axis of the crystal, the magnetic field shows almost negligible influence on the q-FM mode frequency. When the magnetic field is applied along  $c$ -axis for  $\Gamma_4$  phase and along  $c$ -axis for  $\Gamma_2$  phase, the field can lead to softening of the q-FM mode. In addition, the magnetic field along  $a$ -axis can induce the rotation of magnetic moment  $\mathbf{F}$  in  $ac$  plane of the crystal, which could result in the occurrence of the SRT under sufficiently large magnetic field. By consulting the temperature dependent magnetic anisotropic constants,  $A_{xx}$ ,  $A_{zz}$ ,  $A_{xz}$  and  $A_{xy}$ , the mapping of both temperature and magnetic field dependent spin resonance can be obtained with phenomenal analysis. Our studies lead to a more systematic and in-depth understanding of the external field dependent spin resonance as well as the SRT in rare earth orthoferrites.

#### Acknowledgments

This work was supported by the National Natural Science Foundation of China (NSFC, Nos. 11674213, 61975110, 11604202, 61735010, and 11774217). ZJ thanks the Young Eastern Scholar (QD2015020) at the Shanghai Institutions of Higher Learning, Science and Technology Commission of Shanghai Municipality (Shanghai Rising-Star Program 18QA1401700), and Shanghai Educational Development Foundation (Chen Guang project 16CG45).

#### ORCID iDs

Zuanming Jin  <https://orcid.org/0000-0002-9686-7965>  
 Zhigao Sheng  <https://orcid.org/0000-0003-3382-5968>  
 Guohong Ma  <https://orcid.org/0000-0002-3972-5012>

#### References

- [1] Wolf S A, Awschalom D D, Buhrman R A, Daughton J M, Von Molnár S, Roukes M L, Chtchelkanova A Y and Treger D M 2001 Spintronics: a spin-based electronics vision for the future *Science* **294** 1488–95
- [2] Tudosa I, Stamm C, Kashuba A B, King F, Siegmann H C, Stöhr J, Ju G, Lu B and Weller D 2004 The ultimate speed of magnetic switching in granular recording media *Nature* **428** 831–3
- [3] Kimel A V, Ivanov B A, Pisarev R V, Usachev P A, Kirilyuk A and Rasing T 2009 Inertia-driven spin switching in antiferromagnets *Nat. Phys.* **5** 727–31
- [4] De Jong J A, Razdolski I, Kalashnikova A M, Pisarev R V, Balbashov A M, Kirilyuk A, Rasing T and Kimel A V 2012 Coherent control of the route of an ultrafast magnetic phase transition via low-amplitude spin precession *Phys. Rev. Lett.* **108** 157601
- [5] Afanasiev D, Ivanov B A, Kirilyuk A, Rasing T, Pisarev R V and Kimel A V 2016 Control of the ultrafast photoinduced magnetization across the Morin transition in DyFeO<sub>3</sub> *Phys. Rev. Lett.* **116** 097401
- [6] Nova T F, Cartella A, Cantaluppi A, Först M, Bossini D, Mikhaylovskiy R V, Kimel A V, Merlin R and Cavalleri A 2017 An effective magnetic field from optically driven phonons *Nat. Phys.* **13** 132–6
- [7] De Jong J, Kimel A V, Pisarev R V, Kirilyuk A and Rasing T 2011 Laser-induced ultrafast spin dynamics in ErFeO<sub>3</sub> *Phys. Rev. B* **84** 104421
- [8] White R L 1969 Review of recent work on the magnetic and spectroscopic properties of the rare earth orthoferrites *J. Appl. Phys.* **40** 1061–9
- [9] Yamaguchi T 1974 Theory of spin reorientation in rare-earth orthochromites and orthoferrites *J. Phys. Chem. Solids* **35** 479–500
- [10] Zhao W, Cao S, Huang R, Cao Y, Xu K, Kang B, Zhang J and Re W 2015 Spin reorientation transition in dysprosium–samarium orthoferrite single crystals *Phys. Rev. B* **91** 104425
- [11] Dzyaloshinsky I 1958 A thermodynamic theory of ‘weak’ ferromagnetism of antiferromagnetics *J. Phys. Chem. Solids* **4** 241–55
- [12] Moriya T 1960 Anisotropic superexchange interaction and weak ferromagnetism *Phys. Rev.* **120** 91–8
- [13] Liu X M *et al* 2018 Terahertz magnon and crystal-field transition manipulated by  $R^{3+}$ – $Fe^{3+}$  interaction in Sm<sub>0.5</sub>Pr<sub>0.5</sub>FeO<sub>3</sub> *Appl. Phys. Lett.* **113** 022401
- [14] Kimel A V, Kirilyuk A, Usachev P A, Pisarev R V, Balbashov A M and Rasing T 2005 Ultrafast non-thermal control of magnetization by instantaneous photomagnetic pulses *Nature* **435** 655–7
- [15] Kimel A V, Kirilyuk A, Tsvetkov A, Pisarev R V and Rasing T 2004 Laser-induced ultrafast spin reorientation in the antiferromagnet TmFeO<sub>3</sub> *Nature* **429** 850–53
- [16] Chen L, Li T, Cao S, Yuan S, Hong F and Zhang J 2012 The role of 4f-electron on spin reorientation transition of NdFeO<sub>3</sub>: a first principle study *J. Appl. Phys.* **111** 103905
- [17] Wang W B *et al* 2013 Room-temperature multiferroic hexagonal LuFeO<sub>3</sub> films *Phys. Rev. Lett.* **110** 237601
- [18] Ramu N, Muralidharan R, Meera K and Jeong Y H 2016 Tailoring the magnetic and magnetoelectric properties of rare earth orthoferrites for room temperature applications *RSC Adv.* **6** 72295–9
- [19] Xu C, Yang Y, Wang S, Duan W, Gu B and Bellaiche L 2014 Anomalous properties of hexagonal rare-earth ferrites from first principles *Phys. Rev. B* **89** 205122

- [20] Jiang J J, Song G B, Wang D Y, Jin Z M, Tian Z, Lin X, Han J G, Ma G H, Cao S X and Cheng Z X 2016 Magnetic-field dependence of strongly anisotropic spin reorientation transition in NdFeO<sub>3</sub>: a terahertz study *J. Phys.: Condens. Matter* **28** 116002
- [21] Tokunaga Y, Iguchi S, Arima T and Tokura Y 2008 Magnetic-field-induced ferroelectric state in DyFeO<sub>3</sub> *Phys. Rev. Lett.* **101** 097205
- [22] Shen H, Cheng Z, Hong F, Xu J, Yuan S, Cao S and Wang X 2013 Magnetic field induced discontinuous spin reorientation in ErFeO<sub>3</sub> single crystal *Appl. Phys. Lett.* **103** 192404
- [23] Jin Z, Tkach A, Casper F, Spetter V, Grimm H, Thomas A, Kampfrath T, Bonn M, Kläui M and Turchinovich D 2015 Accessing the fundamentals of magnetotransport in metals with terahertz probes *Nat. Phys.* **11** 761–6
- [24] Kampfrath T, Tanaka K and Nelson K A 2013 Resonant and nonresonant control over matter and light by intense terahertz transients *Nat. Photon.* **7** 680–90
- [25] Zhou R, Jin Z, Li G, Ma G, Cheng Z and Wang X 2012 Terahertz magnetic field induced coherent spin precession in YFeO<sub>3</sub> *Appl. Phys. Lett.* **100** 061102
- [26] Mukai Y, Hirori H, Yamamoto T, Kageyama H and Tanaka K 2014 Antiferromagnetic resonance excitation by terahertz magnetic field resonantly enhanced with split ring resonator *Appl. Phys. Lett.* **105** 022410
- [27] Jiang J J, Jin Z M, Song G B, Lin X, Ma G H and Cao S X 2013 Dynamical spin reorientation transition in NdFeO<sub>3</sub> single crystal observed with polarized terahertz time domain spectroscopy *Appl. Phys. Lett.* **103** 062403
- [28] Yamaguchi K, Kurihara T, Minami Y, Nakajima M and Suemoto T 2013 Terahertz time-domain observation of spin reorientation in orthoferrite ErFeO<sub>3</sub> through magnetic free induction decay *Phys. Rev. Lett.* **110** 137204
- [29] Liu X, Jin Z, Zhang S, Zhang K, Zhao W, Xu K, Lin X, Cheng Z, Cao S and Ma G 2018 The role of doping in spin reorientation and terahertz spin waves in SmDyFeO<sub>3</sub> single crystals *J. Phys. D: Appl. Phys.* **51** 024001
- [30] Zhang K, Xu K, Liu X, Zhang Z, Jin Z, Lin X, Li B, Cao S and Ma G 2016 Resolving the spin reorientation and crystal-field transitions in TmFeO<sub>3</sub> with terahertz transient *Sci. Rep.* **6** 23648
- [31] Shapiro S M, Axe J D and Remeika J P 1974 Neutron-scattering studies of spin waves in rare-earth orthoferrites *Phys. Rev. B* **10** 2014–21
- [32] Koshizuka N and Ushioda S 1980 Inelastic-light-scattering study of magnon softening in ErFeO<sub>3</sub> *Phys. Rev. B* **22** 5394–9
- [33] Herrmann G F 1963 Resonance and high frequency susceptibility in canted antiferromagnetic substances *J. Phys. Chem. Solids* **24** 597–606
- [34] Balbashov A M, Kozlov G V, Mukhin A A and Prokhorov A S 1995 Submillimeter spectroscopy of antiferromagnetic dielectrics: rare-earth orthoferrites *High Frequency Processes in Magnetic Materials* ed G Srinivasan and A Slavin (Singapore: World Scientific) part I, pp 56–98
- [35] Li X et al 2018 Observation of Dicke cooperativity in magnetic interactions *Science* **361** 794–7
- [36] Gorodetsky G, Shaft S and Remeika J P 1981 Propagation of surface magnetoelastic waves in TmFeO<sub>3</sub> at the spin reorientation *J. Appl. Phys.* **52** 7353
- [37] Lin X, Jiang J, Jin Z, Wang D, Tian Z, Han J, Cheng Z and Ma G 2015 Terahertz probes of magnetic field induced spin reorientation in YFeO<sub>3</sub> single crystal *Appl. Phys. Lett.* **106** 092403
- [38] Jacobs I S, Burne H F and Levinson L M 1971 Field-induced spin reorientation in YFeO<sub>3</sub> and YCrO<sub>3</sub> *J. Appl. Phys.* **42** 1631–2
- [39] Balbashov A M, Berezin A G, Gufan Yu M, Kolyadko G S, Marchukov P Yu and Rudashevskii E G 1987 Soft mode and energy gap in spin-wave spectrum in a second-order orientational phase transition. AFMR in YFeO<sub>3</sub> *Sov. Phys. JETP* **66** 174–81